

Francesco Bloisi, Carlo Ebanista, Lidia Falcone, Luciano Vicari  
***Infrared image analysis and elaboration for archaeology:  
The case study of a medieval “capsella” from Cimitile, Italy***

[A stampa in “Applied Physics B, Laser and Optics”, 101 (2010), pp. 471-479 © degli autori - Distribuito in formato digitale da “Reti Medievali”, [www.biblioteca.retimedievali.it](http://www.biblioteca.retimedievali.it)].

# Infrared image analysis and elaboration for archaeology: The case study of a medieval “capsella” from Cimitile, Italy

F. Bloisi · C. Ebanista · L. Falcone · L. Vicari

Received: 18 December 2009 / Revised version: 5 March 2010 / Published online: 14 May 2010  
© Springer-Verlag 2010

**Abstract** Infrared reflectography, i.e. the use of images taken with infrared light, is currently applied in the field of cultural heritage mainly for paintings analysis to reveal the presence of underdrawings or alterations. Its use in archaeology for deciphering faded signs (texts, images, tattoos, etc.) is a lot more limited and in most cases no or simple data analysis and elaboration is performed. Here we show that infrared reflectography taken by using a wide spectral response (wavelength range from 400 to 2200 nm) VIDICON image acquisition system together with adequate post-elaboration, taking advantage from advanced techniques for data analysis (wavelet decomposition) and image registration and fusion, is able to produce high-quality ‘C&IR’ images. Such images can be obtained in a relatively easy way using the same hardware configuration generally used for infrared reflectographic analysis of paintings. The application to a medieval *capsella* (a small wooden relics container) from Cimitile, Italy, has shown that these results are of great interest for archaeologists.

## List of Abbreviations

CCD      Charge Coupled Device  
C&IR     Colour & InfraRed fused images

---

F. Bloisi (✉) · L. Vicari  
Dipartimento di Scienze Fisiche, Università di Napoli  
“Federico II”, Napoli, Italy  
e-mail: [bloisi@na.infn.it](mailto:bloisi@na.infn.it)

C. Ebanista  
Dipartimento di Scienze Umane, Storiche e Sociali, Università del  
Molise, Campobasso, Italy

L. Falcone  
Dottore di Ricerca in Archeologia (Archeologia Greca e  
Romana), Caserta, Italy

CIE	Commission Internationale de l’Eclairage
CMYK	A way to represent colours as <b>C</b> yan, <b>M</b> agenta, <b>Y</b> ellow and <b>K</b> ey (i.e. black) channels
DIN	Deutsches Institut für Normung
FITS	Flexible Image Transport System
FPA	Focal Plane Array
IEC	International Electrotechnical Commission
I-IUWT	Iterative-Isotropic Undecimated Wavelet Transform
IR	InfraRed radiation (electromagnetic radiation in the wavelength range 780 nm–1 mm)
IR-A	IR radiation in the wavelength range 780–1400 nm (CIE classification)
IR-B	IR radiation in the wavelength range 1400–3000 nm (CIE classification)
IRR	InfraRed Reflectography
ISO	International Organization for Standardization (from Greek word “ισος”, <b>isos</b> , equal)
IUWT	Isotropic Undecimated Wavelet Transform
Lab	A way to represent colours as <b>L</b> ightness and colour ( <b>a</b> , <b>b</b> ) components, defined by CIE
LCh	A way to represent colours as <b>L</b> ightness, <b>C</b> hroma and <b>h</b> ue, defined by CIE
lRGB	A way to represent colours as <b>l</b> inear <b>R</b> ed, <b>G</b> reen and <b>B</b> lue channels
NIR	Near <b>IR</b> : radiation in the wavelength range 0.75–1.4 μm (DIN classification)
r-IR	reflected <b>IR</b> : IR radiation in the wavelength range below 2500–3000 nm
RoI	Region of Interest within an image
sRGB	A way to represent colours as standard <b>R</b> ed, <b>G</b> reen and <b>B</b> lue channels
SNR	Signal-to-Noise Ratio

SWIR	<b>Short Wavelength IR:</b> radiation in the wavelength range 1.4–3.0 $\mu\text{m}$ (DIN classification)
<i>t</i> -IR	<b>thermal IR:</b> IR radiation in the wavelength range above 2500–3000 nm
UV	<b>UltraViolet</b> radiation (electromagnetic radiation in the wavelength range 10–380 nm)
VIDICON	A camera pickup tube where the image is scanned by an electron beam
VIS	<b>VISible</b> light (electromagnetic radiation in the wavelength range 380–780 nm)

## 1 Introduction

Infrared reflectography [1] (IRR), namely the use of images electronically taken with infrared light, not perceived by human eye, is currently used in the field of cultural heritage mainly for paintings analysis [2, 3] in order to show the presence of underdrawings or alterations. Even if its use in archaeology is much more limited [4, 5], we have recently [6, 7] shown that infrared (IR) radiation in the spectral region up to wavelengths of about 2200 nm allows deciphering ablated text on plaster. Starting from this unexpected but very interesting result we have extended our field of interest to other materials such as wood [5]. The radiation used (900–2200 nm) is within the IR-A (780–1400 nm) and the IR-B (1400–3000 nm) regions [8] of the electromagnetic spectrum and is sometimes called “reflected infrared” (*r*-IR, i.e. infrared radiation *reflected* by objects depending on their surface characteristics) in order to be distinguished from “thermal infrared” (*t*-IR, i.e. infrared radiation *emitted* by objects depending on their surface temperature and characteristics), corresponding to longer (up to 1 mm) wavelengths. A drawback of the wide spectral range used is the lower quality of the infrared images with respect to usual grey-scale or colour images taken with a camera mounting a CCD (Charge Coupled Device) sensor. This is due to several reasons: the lenses used with the IR camera are designed for visible light and are unable to compensate the chromatic aberrations for light in the wide *t*-IR spectral range (this implies the use of a high stop number or to accept partially blurred images); the electronic noise implied in the use of VIDICON (often used to obtain such a wide spectral range) cameras generates images which are more noisy than the images obtained by usual CCD based digital cameras. High-resolution, low SNR (Signal-to-Noise Ratio) reflectographic images can be obtained using an FPA (Focal Plane Array) detector [9] and high-quality wide spectral range (200–5000 nm, i.e. from UV to IR) images (called *reflectoscopy* [10]) can be obtained recording, for each pixel the reflectance spectrum, but both such techniques cannot be widely applied due to their cost and non-commercial availability. Often simple infrared reflectography (i.e. limited to

the IR-A range), is used [11] for individuating small areas to be examined in more detail with sophisticated physical or chemical analyses. Even off-the-shelf or slightly modified professional or consumer digital still cameras [4] can be used to obtain a limited IR recording capability. However, the “classical” infrared reflectographic systems based on VIDICON tubes are still the ones most used. Here we show that a VIDICON based wide spectral range (900–2200 nm) infrared reflectography, together with appropriate data analysis allows recovering obscured text from a small wooden artefact. The use of wavelet analysis [12], an evolution of Fourier analysis, for data (in our case images) examination often allows to extract information otherwise masked by noise [13]. Taking advantage from wavelet-data analysis and applying image registration and fusion techniques, we will be able to obtain good quality colour image containing relevant information from infrared image. In the following, after a brief survey of current applications of infrared reflectography in archaeology, we will discuss the way to examine infrared and visible data in order to increase the amount of information of interest the archaeologists can obtain. Finally we briefly discuss the results obtained in the case studied (a *capsella*, a small wooden container for relics, from Cimitile, Italy). On the bottom external surface there is some text partially visible to the naked eye. Reading the text is of great interest for archaeologists since it can allow the correct attribution of relics originally contained in the *capsella*, thus supplying additional information concerning the history of the *Complesso Basilicale* medieval archaeological site [14–16].

## 2 Infrared reflectography

Infrared reflectography, an evolution of infrared photography introduced in the 1960s by Van Asperen de Boer [1, 2], is a non-destructive imaging technique used in order to get information unobtainable with visual (or photographic) inspection. The infrared (IR) range of the electromagnetic spectrum is the region between visible light (following CIE [8], visible light wavelengths (VIS) range from 380 to 780 nm) and microwaves (wavelengths from 1 mm up to 1 m). The IR range is therefore so wide (780 nm–1 mm) that physical, physiological and biological effects are quite different and therefore several sub-ranges have been defined. Here we are interested in distinguishing between the so called “reflected-IR” (*r*-IR) and “thermal-IR” (*t*-IR) since only the first (up to the absorption of CO<sub>2</sub> molecules at 2500–3000 nm) can be used in reflectography (which uses infrared radiation *reflected* by the object in order to get information on its composition up to some depth from surface) while the latter is used by thermography (which uses infrared radiation *emitted* by the object as an indication of its

temperature and surface emission characteristics). The  $r$ -IR wavelengths correspond to IR-A and IR-B (following CIE classification [8]) or to NIR and SWIR (following DIN classification [17]).

Despite reflectography is currently a well-established technique, from a methodological and theoretical point of view, used in the study of paintings, it is not widely employed in archaeology. In most cases the examined situations are new due to the nature of materials (substrate, pigments, binders, etc.) and the goal of the study (revealing faded or low contrast signs). We can state that reflectography is routinely used in painting analysis while it only finds seldom experimental applications in archaeology.

Infrared reflectographic technique for paintings examination is based on the different optical behaviour of pictorial layers to VIS and  $r$ -IR wavelengths. This effect is a consequence of both lower absorption of the pigment and reduced scattering due to pigment particle size smaller than infrared wavelengths.

More generally, the difference between a VIS and a  $r$ -IR image is that the two images contain information from a different region of the spectrum and from a different depth from the surface. In addition  $r$ -IR images can also register radiation emitted by the object due to fluorescence. This allows a somewhat different use of reflectography in order to reveal signs not recognisable in VIS images due to several reasons, especially for texts written on soft (parchment, papyrus, leather, textiles and also wood) materials that are easily deteriorated with a consequent high degradation of the text. In fact, typically used in writing such documents it is often faded and results indistinguishable from darkened aged surfaces. Even if this application is of high interest in archaeology, it is less studied from a theoretical point of view and seldom applied.

Some archaeological applications of IR photography/reflectography concern the Dead Sea Scrolls [18], the carbonised papyri from *Villa dei Papiri* in Herculaneum and from Petra in Jordan [19], the Papyrus of Posidippus [20, 21], the written tablets from Roman site of Vindolanda in Great Britain [22], the tattoos on a mummified human body from Nubian necropolis in Sudan [23], the notice board on the *castellum aquae* in Herculaneum [7]. In all cases the results have been of great archaeological interest, even if, in most cases, the IR images are used “as they are” or with little elaboration.

### 3 Image acquisition and elaboration

Infrared images are often quite difficult to be interpreted, due to several reasons (low spatial resolution, high aberrations, simultaneous presence of information from visible image, etc.). In this section we illustrate the procedure followed in order to get final image (let us call it C&IR) shown

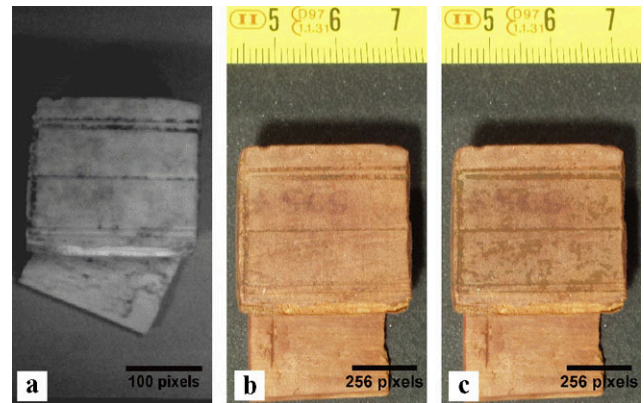


**Fig. 1** The original infrared **a** and colour **b** images used to generate the C&IR image **c** shown on the *right*

in Fig. 1c, starting with an infrared (Fig. 1a) and a colour (Fig. 1b) image. The C&IR image is perceptually similar to a colour image (has the same resolution, chromatic information, etc.) but also contains relevant information taken from the infrared image, so that its information content is somewhat greater than the information content of colour and infrared images observed separately.

#### 3.1 Infrared image

The infrared image shown in Fig. 1a has been taken using a Hamamatsu system [24] (VIDICON camera head C2741-03D with a camera controller C2471) mounting Nikon objectives. An optical-filter cutting wavelengths shorter than 900 nm is used to exclude visible radiation (high band-pass Hoya RM90 [25] Infrared Transmitting Filter). The camera has been chosen since it has a wide spectral response (wavelength range from 400 to 2200 nm). The specimen, a medieval *capsella* [5], is illuminated using a specific tungsten filament lamp with coloured bulb in order to partially filter visible radiation. The images are both displayed on a monitor for direct visual inspection and digitally recorded (768 × 576 pixels, 256 grey levels) on a portable computer. Images are stored on the field as bitmap files but, in view of subsequent elaborations, are converted to FITS (Flexible Image Transport System) formatted files [26, 27] since this format, widely used in astronomy, is characterised by a great flexibility and is composed by a text formatted header followed by raw image data stored as integer (up to 32 bit) or float (up to 64 bit) values.

Main disadvantages of the VIDICON infrared systems are image persistence and image distortion. The first issue is of no importance for still images, while the second requires some care in verifying the effect of the specific objective/camera combination. It is possible to apply specific techniques in order to detect and correct optical distortions [28, 29] but here we are interested in detecting the presence

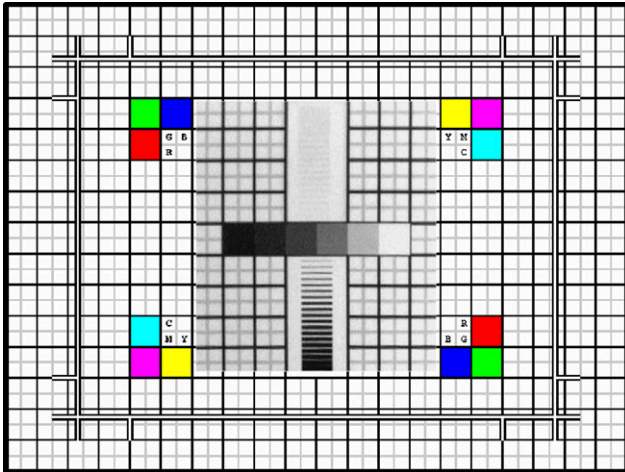


**Fig. 2** The test pattern used to verify image distortion introduced by the VIDICON camera: both black and grey lines are 0.5 mm thick, thick marked squares are 1 cm × 1 cm. Central ~8 cm × ~9 cm area has been replaced with the central area of the image taken with the VIDICON camera

of relatively large “signs” so, before taking the image of the “capsella” shown in Fig. 1a we have simply taken the image of a test pattern placed in place of the sample. In Fig. 2 the central area (421 × 432 pixels, corresponding to slightly less than 8 cm × 9 cm) of such image has been superimposed to the original image, showing that distortion in the zone where is positioned the 216 × 162 pixels RoI (Region of Interest) used for subsequent image analysis is negligible since is largely within the size of the text we are looking for.

Subsequent procedures require image data being proportional to scattered light intensity. Some care must be applied in interpreting data stored in image files: such data are usually ready to be displayed, i.e. are split into Red/Green/Blue channels and include a “gamma factor” [30] used to take into account non-linear response of both reproduction media and human eye.

In order to linearise the image data we convert *s*RGB [31] representation (infrared images are stored as grey levels, i.e. *s*RGB images with Red, Green and Blue components having the same value:  $R_s = G_s = B_s = I_s$ ) to CIE- $L^*a^*b^*$  [32] representation (obviously for a greyscale image  $a^* = b^* = 0$ , see the following subsection for more details concerning *s*RGB and CIE- $L^*a^*b^*$  colour representations) so that (here and in the following,  $L^*$  is normalised to the [0.0, 1.0] range and not [0, 100] as usual):

$$L^* = (1 + L_0)f_1(Y) - L_0 \tag{1}$$

where

$$L_0 = 0.16$$

$$f_1(Y) = \begin{cases} k_1 Y + k_0 & \text{for } Y \leq Y_0 \\ Y^{1/3} & \text{for } Y > Y_0 \end{cases}$$

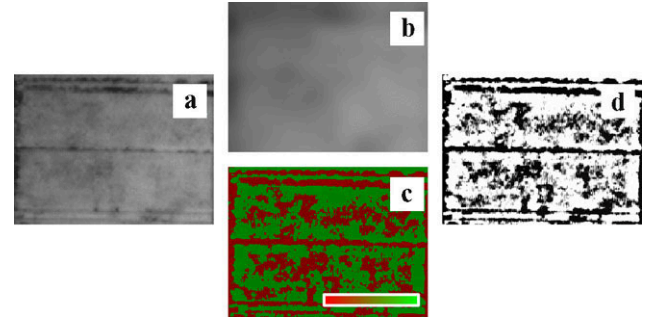


**Fig. 3** The RoI extracted from infrared image **a** is decomposed into background **b** and foreground **c** images applying the Iterative Isotropic Undecimated Wavelet Transform (I-IUWT) described in the text. Pixels in foreground image can be both positive (lighter than background, represented in green) or negative (darker than background, represented in red). The enhanced image **d** is obtained increasing the contrast of the foreground image and decreasing the contrast of the background image before recombination

$$Y_0 = 0.008856$$

$$k_0 = \frac{L_0}{L_0 + 1}; \quad k_1 = \frac{Y_0^{1/3} - k_0}{Y_0}$$

$$f_{\gamma,a_0}^{-1}(I_s) = \begin{cases} \left(\frac{I_s+d}{1+d}\right)^{1/\gamma} & \text{for } I_s \leq sa_0 \\ \frac{I_s}{s} & \text{for } I_s > sa_0 \end{cases} \tag{2}$$

$$\gamma = 1/2.4; \quad a_0 = 0.00304$$

$$s = \frac{\gamma}{a_0(\gamma - 1) + a_0^{1-\gamma}}; \quad d = \frac{1}{a_0^\gamma(\gamma - 1) + 1} - 1$$

Following a visual comparative inspection of the infrared and the colour image, a RoI is selected (Fig. 3a) containing the relevant information: in our case the RoI is the surface containing the two “text lines” where in the infrared image some text, not detectable in colour image or by direct visual inspection, can be guessed.

In analysing images of archaeological findings and in the case we are studying we are mainly interested in separating image background in order to increase visibility of obscured text. To this aim the Iterative Isotropic Undecimated Wavelet Transform (I-IUWT) is defined and carried out. The result is a decomposition of the linearised object image into a couple of images we call “background” and “foreground” object images.

The I-IUWT is the result of iterative application of a single step IUWT (Isotropic Undecimated Wavelet Transform) [33] to the smoothed image resulting from previous iteration. A single step IUWT decompose the original reference image into low spatial frequencies (smoothed) image and high spatial frequencies (detail) image applying the filters

$$h[k, l] = h^{(1D)}[k]h^{(1D)}[l]$$

$$g[k, l] = \delta[k, l] - h[k, l]$$

where

$$h^{(1D)}[m] = \frac{[1, 4, 6, 4, 1]}{16} \quad m = -2, -1, 0, +1, +2$$

corresponds to a  $B^3$ -Spline in one dimension and  $\delta$  is zero with the exception of  $\delta[0, 0] = 1$ .

If  $\mathcal{C} = \{c_0[m, n]\}$  are object image data, then at  $j$ -th iteration of the single step IUWT we get a smoothed image  $\mathcal{S}_j = \{c_j[m, n]\}$  performing the convolution with the filter  $h[k, l]$

$$c_j[m, n] = \sum_{k,l=-2}^{+2} h[k, l]c_{j-1}[m - k, n - l]$$

and a detail image  $\mathcal{D}_j = \{d_j[m, n]\}$  performing the convolution with the filter  $g[k, l]$

$$d_j[m, n] = \sum_{k,l=-2}^{+2} g[k, l]c_{j-1}[m - k, n - l]$$

The definition of  $g[k, l]$  allows to write the detail image as the difference

$$d_j[m, n] = c_j[m, n] - c_{j-1}[m, n]$$

between two subsequent iterations (let us assume, for  $j = 0$ ,  $\mathcal{S}_0 = \mathcal{C}$ ).

The background image  $\mathcal{B} = \{b[m, n]\}$  (Fig. 3b) is the result of last iteration

$$b[m, n] = c_J[m, n]$$

while the foreground image  $\mathcal{F} = \{f[m, n]\}$  (Fig. 3c) is the sum of all detail images

$$f[m, n] = \sum_{j=1}^J d_j[m, n] = c_J[m, n] - c_0[m, n]$$

so that the original image can be reconstructed as the sum of foreground and background

$$c_0[m, n] = f_J[m, n] + b_J[m, n]$$

Note that the I-IUWT is not the same as the *à trous* [34] wavelet transform, since we apply exactly the same filter at each iteration (without inserting the “holes” characterising the *à trous* transform). The reason is that we want to extract image background instead of performing a separation of different levels of detail.

Since the information we want to extract from infrared image are contained in the foreground image we enhance its contrast while reducing the contrast of background image before recomposing them in order to get the enhanced infrared image (Fig. 3d). This is the NIR image we will use.

### 3.2 Colour image

The colour image shown in Fig. 1b has been taken with an *Olympus  $\mu$ -mini digital* camera able to acquire images with  $2272 \times 1704$  pixels, 16 777 216 colours, using a couple of halogen lamps to illuminate the finding.

In order to carry out infrared and colour images fusion we select and extract from the colour image a RoI (Fig. 4a) as similar as possible to the corresponding one already selected in the infrared image.

Colour images are usually stored in a “ready to display” format, i.e. representing pixel information as will be displayed on a monitor, in *sRGB* [31] (standard Red/Green/Blue) mode.

Even if *sRGB* is useful in displaying images there are several other possible representations. For example, images to be printed are usually represented as *CMYK* (Cyan/Magenta/Yellow/Key colour or black) [35]. The necessity of being able to reproduce the same image on different devices or supports has lead to the requirement of a general representation of colours. A device independent way of representing colours is *CIE- $L^*a^*b^*$*  (or, equivalently,  *$L^*C_{ab}h_{ab}$* ) [32]. It is very general since it is oriented to simulate the human eye physiology and is the most apt to subsequent elaborations. In this representation, for each pixel of the image,  $L^*$  is its *Lightness*,  $C_{ab}$  is its *Chroma*, i.e. colour saturation, and  $h_{ab}$  (usually measured in degrees) is its *Hue* ( $0^\circ$  corresponding to red/magenta,  $90^\circ$  to yellow,  $180^\circ$  to green,  $270^\circ$  to blue). In this colorimetric coordinates representation, selecting the  $L^*$  component alone, i.e. fixing  $a^* = b^* = 0$  or  $C_{ab} = 0$  ( $h_{ab}$  is undetermined) we get a “grey level” image (let us call it the *VIS* image) which, after fusion with the *NIR* image, will be reconverted to a

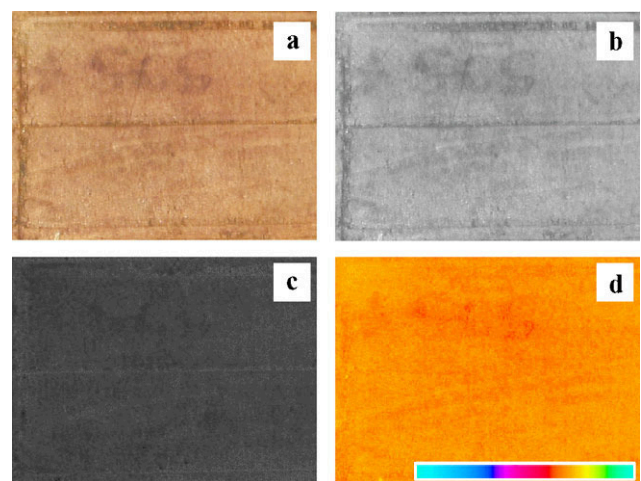


**Fig. 4** The RoI extracted from the colour image **a** and its representation in *CIE- $L^*C_{ab}h_{ab}$*  colour coordinates: lightness **b**, chroma **c** and hue **d**. The look-up table used to represent hue in the range  $[-180^\circ, +180^\circ]$  is also shown

colour image by adding the colour information contained in  $C_{ab}$  and  $h_{ab}$  components.

The fundamental colour representation stated by CIE is given in terms of the *tristimulus values* ( $X, Y, Z$ ) [36] mimicking the response of the human eye to a given colour characterised by the spectral power distribution  $I(\lambda)$ :

$$X = \int_0^\infty I(\lambda)\bar{x}(\lambda) d\lambda$$

$$Y = \int_0^\infty I(\lambda)\bar{y}(\lambda) d\lambda$$

$$Z = \int_0^\infty I(\lambda)\bar{z}(\lambda) d\lambda$$

where  $\bar{x}(\lambda), \bar{y}(\lambda)$  and  $\bar{z}(\lambda)$  are the CIE-defined colour-matching functions.

The conversion from linear ( $IRGB$ ) representation is given, in matrix representation, by

$$\begin{bmatrix} X \\ Y \\ Z \end{bmatrix} = \frac{1}{b_{21}} \begin{bmatrix} b_{11} & b_{12} & b_{13} \\ b_{21} & b_{22} & b_{23} \\ b_{31} & b_{32} & b_{33} \end{bmatrix} \cdot \begin{bmatrix} R \\ G \\ B \end{bmatrix}$$

with  $b_{11} = 0.49, b_{12} = 0.31, b_{13} = 0.20, b_{21} = 0.17697, b_{22} = 0.81240, b_{23} = 0.01063, b_{31} = 0.00, b_{32} = 0.01, b_{33} = 0.99$  while the removal of the ‘‘gamma correction’’ to convert non-linear  $sRGB$  to linear  $IRGB$  representation is given by [30]:

$$R = f_{\gamma,a_0}^{-1}(R_s), \quad G = f_{\gamma,a_0}^{-1}(G_s), \quad B = f_{\gamma,a_0}^{-1}(B_s)$$

where  $f_{\gamma,a_0}^{-1}$  is the function already defined in (2).

CIE- $L^*a^*b^*$  or CIE- $L^*C_{ab}h_{ab}$  colour coordinates are given by (1) and

$$a^* = a_0(f_1(X/X_{ref}) - f_1(Y/Y_{ref}))$$

$$b^* = b_0(f_1(Y/Y_{ref}) - f_1(Z/Z_{ref}))$$

where

$$a_0 = 500/127, \quad b_0 = 200/127$$

and, for D65 (Daylight 6500 K, i.e. a blackbody at temperature 6500 K, similar to sunlight) illuminant,

$$X_{ref} = 0.950456,$$

$$Y_{ref} = 1.0,$$

$$Z_{ref} = 1.088754$$

and

$$C_{ab} = \sqrt{a^{*2} + b^{*2}}$$

$$h_{ab} = (1/\pi)\tan^{-1}(b^*/a^*)$$

Here  $a^*$  and  $b^*$  are normalised to  $[-1.0, +1.0]$  (instead of  $[-127, +127]$  as usual) so that  $C_{ab}$  is in the range  $[0.0, 1.0]$  (instead of  $[0, 100]$  as usual) and  $h_{ab}$  is normalised to the range  $[-1.0, +1.0]$  (instead of  $[0^\circ, 360^\circ]$  as usual).

The choice between Cartesian ( $a^*, b^*$ ) and polar ( $C_{ab}, h_{ab}$ ) representation of colour coordinates is just for convenience of visual representation:  $a^*$  and  $b^*$  mix colours together (green/red-magenta and blue/yellows respectively), while only  $h_{ab}$  contains colour information. The ROI extracted from colour image is shown in Fig. 4a together with its representation in CIE- $L^*C_{ab}h_{ab}$  components: Lightness (Fig. 4b), Chroma (Fig. 4c) and Hue (Fig. 4d).

Due to VIDICON cameras characteristics NIR image has generally a lower resolution ( $\sim 80$  pixel/cm for image in Fig. 1a) than the one of the VIS image taken with a CCD ( $\sim 250$  pixel/cm for image in Fig. 1b). In order to carry out fusion of the two images it is necessary to reduce the resolution of the VIS image to the resolution of the NIR image. The resolution can be reduced in a lossless way (i.e. maintaining the information required to revert the procedure after ‘‘fusion’’) adopting a wavelet-based pyramid [37] decomposition. Starting with one ‘‘High-resolution’’  $m \times n$  pixel image, a set of four ‘‘low-resolution’’ ( $m/2 \times n/2$  pixel) images is obtained so that the first (e.g. Fig. 5a) is a lower-resolution version of the original image and the other three images (e.g. Fig. 5b, c, d) contain the details required to revert the process. This procedure can be obviously iterated as required. With the images under consideration just one step (from  $\sim 250$  to  $\sim 125$  pixel/cm, as shown in Fig. 5) is required to obtain an image with resolution comparable to infrared image ( $\sim 80$  pixel/cm): there is no need for an exact match since the subsequent registration can perform a scaling of the image.

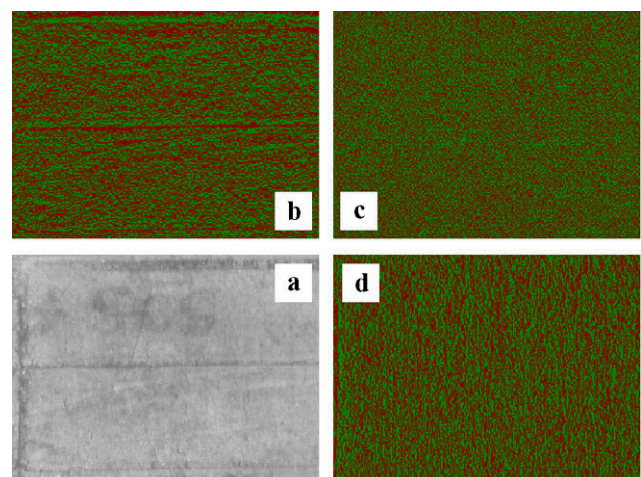


**Fig. 5** The lightness component of the ROI extracted from the colour image is decomposed into a lower-resolution image **a** and the details **b, c** and **d** required to reconstruct the higher resolution image

### 3.3 Image registration and fusion

At this point we have two grey-scale images, the VIS and the NIR images, having the same or at least comparable resolutions, carrying information from the colour and the infrared images respectively.

Usual image registration techniques [38] allows for the determination of a geometrical transformation that aligns points in one image of an object with corresponding points of another image of the same object.

Since the object in the two images (VIS and NIR) to be registered is rigid, the only changes between them are due to difference in the point of view and in the characteristics of the two cameras.

Therefore non-rigid transformations can be limited to scaling and perspective ones so that, using the homogeneous coordinates, the more general transformation we need can be written as [39]

$$\begin{bmatrix} u'_1 \\ u'_2 \\ u'_3 \\ u'_4 \end{bmatrix} = \begin{bmatrix} a_{11} & a_{12} & a_{13} & t_1 \\ a_{21} & a_{22} & a_{23} & t_2 \\ a_{31} & a_{32} & a_{33} & t_3 \\ p_1 & p_2 & p_3 & \alpha \end{bmatrix} \cdot \begin{bmatrix} u_1 \\ u_2 \\ u_3 \\ 1 \end{bmatrix}$$

where  $x = u_1$ ,  $y = u_2$ ,  $z = u_3$  are original coordinates,  $x' = u'_1/u'_4$ ,  $y' = u'_2/u'_4$ ,  $z' = u'_3/u'_4$  are transformed coordinates  $a_{ij}$  are matrix elements containing information concerning scaling and rotation,  $t_i$  are matrix elements containing information concerning translation and  $p_j$  and  $\alpha$  are matrix elements containing information concerning perspective transformation.

Several software tools are currently available in order to determine the coefficients. Our choice has been for ElastiX [40] since it can be easily adapted to manage FITS files and is able to generate the registered image. In Fig. 6 the registered infrared (Fig. 6b) image is shown together with the  $L^*$  component of the colour image (Fig. 6a). Image fusion [41] can be applied to these images, as shown in Fig. 6c. An inhomogeneous transparency can be adopted in order to avoid unwanted and fastidious boundary effects when the ROI in reinserted in the original image.

### 3.4 C&IR image generation

Carrying out, inverted and in reverse order [high-resolution image reconstruction (Fig. 7a), CIE- $L^*a^*b^*$  to sRGB conversion, sRGB channels composition (Fig. 7b), ROI reinsertion into image], the same steps performed for obtaining the Lo-res  $L^*$ -component of the colour image ROI we obtain the C&IR image (Fig. 1c), i.e. a high-resolution high-quality colour image containing the desired information from the near-infrared image.

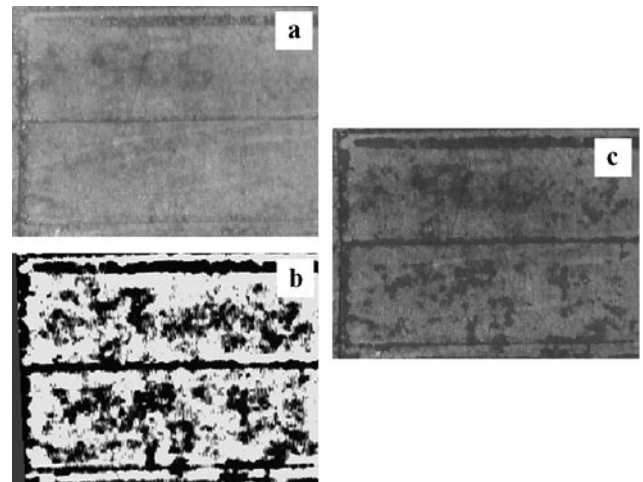


**Fig. 6** The low-resolution (visible) image obtained by pyramid decomposition **a** used as fixed image for registration of infrared enhanced image (Fig. 2d), the registered image **b** and the result of image fusion **c**

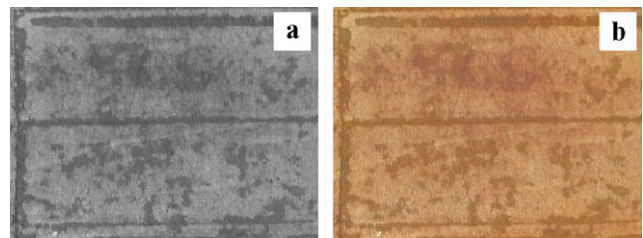


**Fig. 7** The high-resolution (visible and infrared) image obtained after pyramid reconstruction **a** is used as lightness to generate C&IR image **b**

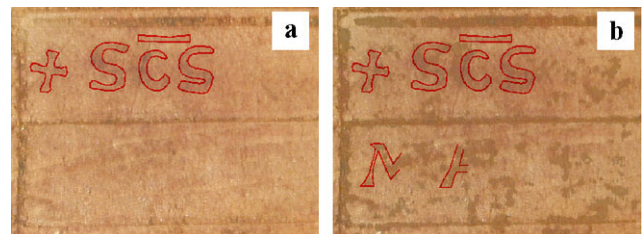


**Fig. 8** The text ‘+ S[AN]C[TU]S’ and ‘MA[...]’ is outlined over the colour **a** and the C&IR **b** images of the outer bottom surface of the capsella

## 4 The case study: a wooden capsella

The examined finding, a *capsella* [42], is a small wooden box (2.5 cm × 2.5 cm, maximum actual height 1.6 cm) obtained from a single wood block and closed by a rectangular (1.6 cm × 2.1 cm) lid. Inner surfaces are rough while outer ones have been smoothed [43]. On the outer bottom surface there is some text written with black ink, delimited by parallel engraved lines, originally on two rows: the upper row contains the visible text ‘+ SCS’, an abbreviation for *sanctus*, i.e. ‘saint’, while the lower row just shows a few



ink traces. Reading the whole text is of great archaeological interest since it could allow the correct attribution of the relics originally contained in the *capsella* and supply useful data concerning the history of the Basilica complex of Cimitile, Italy. The *capsella*, preserved in the *Antiquarium* of the complex, was discovered in 1955 during the demolition of the altar of the St. Felix basilica, together with four other specimens containing minute fragments of bone.

Comparison between colour image (Fig. 1b) and final C&IR image (Fig. 1c) shows that IR reflectography and subsequent data analysis and elaboration has allowed deciphering the text ‘MA[...]’ on the lower row. Even if partial, this result is of great interest since such text, together with the ‘+’ sign and the abbreviation for *sanctus*, seem to allude to the presence of relics of St. Maximus, bishop of Nola at the end of third century. More details on the interpretation of the images from an archaeological point of view can be found elsewhere [5].

## 5 Conclusions

Infrared reflectography is seldomly used in archaeology and in most cases no or simple data analysis and elaboration is performed. Advanced and more expensive techniques (e.g. multispectral images) are generally reserved for few objects of wide interest. Here we have shown that infrared reflectography together with adequate post-elaboration, taking advantage from advanced techniques for data analysis and image registration and fusion, is able to produce high-quality C&IR images. Such images can be obtained in a relatively easy way using the same hardware configuration generally used for infrared reflectographic analysis of paintings. The application to a wooden *capsella* from Cimitile, Italy, has shown that these results are of great interest for archaeologists. We hold for certain that an extensive application of the “classical” infrared reflectography (taken with intermediate level devices currently typically used for painting analysis) coupled with image analysis and elaboration techniques (borrowed from space and medical image analysis) will give results of great interest for archaeologists, with a relatively low cost.

**Acknowledgements** Work partially supported by CRdC “Innova” [44]. The authors want to acknowledge the collaboration of Dr. Giuseppe Vecchio (Soprintendenza Speciale per i beni Archeologici di Napoli e Pompei) [45], Dr. Antonia Solpietro (Diocesi di Nola, Ufficio Beni Culturali) [46], Arch. Michele Papa and Dr. Arcangelo Riccardo (Comune di Cimitile) [47].

The authors state that, even though the whole work is the result of a complete collaboration, it is due to the individuals in the following measure: “Infrared Reflectography” (LF), “Images acquisition and elaboration” (FB), “The case study: a wooden capsella” (CE).

## References

1. J.R.J. van Asperen de Boer, *Stud. Conserv.* **11**, 45 (1966). <http://www.jstor.org/stable/1505404>
2. J.R.J. van Asperen de Boer, *Appl. Opt.* **7**, 1711 (1998). doi: [10.1364/AO.7.001711](https://doi.org/10.1364/AO.7.001711)
3. J.R.J. van Asperen de Boer, *Stud. Conserv.* **14**, 96 (1969). <http://www.jstor.org/stable/1505392>
4. G. Verhoeven, *J. Archaeol. Sci.* **35**, 3087 (2008). doi: [10.1016/j.jas.2008.06.012](https://doi.org/10.1016/j.jas.2008.06.012)
5. C. Ebanista, L. Falcone, F. Bloisi, L. Vicari, The use of infrared images in archaeology: application to a medieval “capsella” from Cimitile, Italy (in preparation)
6. L. Falcone, F. Bloisi, V. Califano, M. Pagano, L. Vicari, *J. Phys. D Appl. Phys.* **40**, 5547 (2007). doi: [10.1088/0022-3727/40/18/006](https://doi.org/10.1088/0022-3727/40/18/006)
7. L. Falcone, F. Bloisi, V. Califano, M. Pagano, L. Vicari, *J. Archaeol. Sci.* **35**, 1708 (2008). doi: [10.1016/j.jas.2007.11.020](https://doi.org/10.1016/j.jas.2007.11.020)
8. CIE (Commission Internationale de l’Eclairage) at <http://www.cie.co.at>, accessed 2 March 2010 and IEC (International Electrotechnical Commission) <http://www.iec.ch>, accessed 2 March 2010, *International Lighting Vocabulary*, 4th edn. (Bureau Central de la Commission Electrotechnique Internationale, Geneva, 1987); ISBN: 9783900734077
9. G. Karagiannis, C. Salpistis, G. Sergiadis, Y. Chryssoulakis, *Rev. Sci. Instrum.* **78**, 065112 (2007), 7 pages. doi: [10.1063/1.2744236](https://doi.org/10.1063/1.2744236)
10. L. Consolandi, D. Bertani, *Infrared Phys. Technol.* **49**, 239 (2007). doi: [10.1016/j.infrared.2006.06.031](https://doi.org/10.1016/j.infrared.2006.06.031)
11. L. Bonizzoni, S. Caglio, A. Galli, G. Poldi, *Appl. Phys. A: Mater. Sci. Process.* **92**, 203 (2008). doi: [10.1007/s00339-008-4482-6](https://doi.org/10.1007/s00339-008-4482-6)
12. S.G. Mallat, *A Wavelet Tour of Signal Processing* (Academic Press, San Diego, 1999); ISBN: 9780124666061; available online at <http://science-direct.com/science/book/9780124666061>
13. M. Lang, H. Guo, J.E. Odegard, C.S. Burrus, R.O. Wells Jr, *IEEE Signal Process. Lett.* **3**, 10 (1996). doi: [10.1109/97.475823](https://doi.org/10.1109/97.475823)
14. *Memorie dell’Accademia di Archeologia, Lettere e Belle Arti in Napoli*, XV (Napoli, 2003)
15. C. Ebanista, F. Fusaro, *Nuova edizione ampliata e aggiornata* (Nola, 2005)
16. C. Ebanista, *Coemeterium*, 4 (Marigliano, 2006)
17. DIN (Deutsches Institut für Normung, <http://www.din.de>) Standard 5031-7
18. L. Schiffman, *Reclaiming the Dead Sea Scrolls* (Doubleday, New York, 1995)
19. D.M. Chabries, S.W. Booras, G.H. Bearman, *Antiquity* **77**, 359 (2003)
20. G. Bastianini, C. Gallazzi, *Posidippo di Pella. Epigrammi* (Università degli Studi di Milano, Milano, 2001)
21. G. Bastianini, A. Casanova, *Atti del Convegno internazionale di studi*, Firenze 13–14 giugno 2002
22. M. Terras, P. Robertson, *J. Inform. Technol. Stud. Human Sci.* **7**, 1 (2005). Available on-line at <http://etjanst.hb.se/bhs/ith/3-7/mtrp.pdf> (accessed 2 March 2010)
23. A. Alvrus, D. Wright, C. Merbs, *J. Archaeol. Sci.* **28**, 395 (2001). doi: [10.1006/jasc.2000.0596S0305-4403\(00\)90596-X](https://doi.org/10.1006/jasc.2000.0596S0305-4403(00)90596-X)
24. Hamamatsu Infrared Camera C2741-03; datasheet available at <http://sales.hamamatsu.com/assets/pdf/hpspdf/C2741-03HPD.pdf> (accessed 2 March 2010)
25. Hoya Optical Filter RM90; datasheet available at <http://www.hoyaoptics.com/pdf/RM90.pdf> (accessed 2 March 2010)
26. D.C. Wells, E.W. Greisen, R.H. Harten, *Astron. Astr. Suppl. Ser.* **44**, 363 (1981). URL: <http://adsabs.harvard.edu/abs/1981A%26AS...44..363W> (accessed 2 March 2010)
27. R.J. Hanisch, A. Farris, E.W. Greisen, W.D. Pence, B.M. Schlesinger, P.J. Teuben, R.W. Thompson, A. Warnock III, *Astron. Astrophys.* **376**, 359 (2001). doi: [10.1051/0004-6361:20010923](https://doi.org/10.1051/0004-6361:20010923)
28. J. Weng, P. Cohen, M. Herniou, *IEEE Trans. Pattern Anal. Mach. Intell.* **14**, 965 (1992). doi: [10.1109/34.159901](https://doi.org/10.1109/34.159901)

29. J.P. de Villiers, F.W. Leuschner, R. Geldenhuys, Proc. SPIE **7266**, 726612 (2008). doi:[10.1117/12.804771](https://doi.org/10.1117/12.804771)
30. W. Burger, M.J. Burge, *Digital Image Processing* (Springer, New York, 2008). ISBN: 9781846283796
31. International standard IEC 61966-2-1:1999 available from International Electrotechnical Commission at <http://www.iec.ch> (accessed 2 March 2010)
32. Joint ISO/CIE Standard ISO 11664-4:2008/CIE S 014-4/E:2007 available from International Organization for Standardization at <http://www.iso.org> (accessed 2 March 2010) or from Commission Internationale de l’Eclairage at <http://www.cie.co.at> (accessed 2 March 2010)
33. J.L. Stark, F. Murtagh, *Astronomical Image and Data Analysis* (Springer, Berlin, 2006). ISBN: 9783540330240
34. M.J. Shensa, IEEE Trans. Signal Process. **40**, 2464 (1992). doi:[10.1109/78.157290](https://doi.org/10.1109/78.157290)
35. G. Sharma (ed.), *Digital Color Imaging Handbook* (CRC Press, Boca Raton, 2003). ISBN: 084930900X
36. H.S. Fairman, M.H. Brill, H. Hemmendinger, Color Res. Appl. **22**, 11 (1997). doi:[10.1002/\(SICI\)1520-6378\(199702\)22:1<11::AID-COL4>3.0.CO;2-7](https://doi.org/10.1002/(SICI)1520-6378(199702)22:1<11::AID-COL4>3.0.CO;2-7)
37. S.G. Mallat, IEEE Trans. Pattern Anal. Mach. Intell. **11**, 674 (1989). doi:[10.1109/34.192463](https://doi.org/10.1109/34.192463)
38. B. Zitová, J. Flusser, Image Vis. Comput. **21**, 977 (2003). doi:[10.1016/S0262-8856\(03\)00137-9](https://doi.org/10.1016/S0262-8856(03)00137-9)
39. J.M. Fitzpatrick, D.L.G. Hill, C.R. Maurer Jr., in *Handbook of Medical Imaging*, ed. by J.M. Fitzpatrick, M. Sonka. Medical Image Processing and Analysis, vol. 2 (SPIE Optical Engineering Press, Bellingham, 2000). ISBN: 0819436224, Chap. 8
40. The software package elastix is freely available from <http://elastix.isi.uu.nl>
41. G. Piella, Information Fusion **4**, 259 (2003). doi:[10.1016/S1566-2535\(03\)00046-0](https://doi.org/10.1016/S1566-2535(03)00046-0)
42. B. Montecvecchi, in *Suppellettile ecclesiastica*, ed. by B. Montecvecchi, S. Vasco Rocca. Dizionario terminologici, vol. 4 (Ministero per i Beni Culturali e Ambientali, Firenze, 1988), pp. 97–205
43. C. Ebanista, in *La parrocchiale di S. Felice nel complesso basilicale di Cimitile*, ed. by C. Ebanista (Coemeterium, 1), pp. 235–243 (Napoli, 1999)
44. Innova: Centro Regionale di Competenza per lo sviluppo ed il trasferimento dell’innovazione applicata ai beni culturali ed ambientali. <http://www.innova.campania.it> (accessed 2 March 2010)
45. <http://www.pompeisites.org> (accessed 2 March 2010)
46. <http://www.diocesiinola.it/?q=node/61> (accessed 2 March 2010)
47. <http://www.comune.cimitile.na.it> (accessed 2 March 2010)